Scientific Visualization, 2025, volume 17, number 3, pages 67 - 76, DOI: 10.26583/sv.17.3.07

Study of a Shock Wave Turbulent Boundary Layer Interaction by Means of Optical Methods

S.S. Popovich[1,A], I.A. Znamenskaya[2,B], M.I. Muratov[3,B], I.A. Zagainov[4,A]

[A] Institute of Mechanics, Lomonosov Moscow State University, Moscow, Russia
[B] Faculty of Physics, Lomonosov Moscow State University, Moscow, Russia

[1] ORCID: 0000-0001-8904-7283, pss@imec.msu.ru
[2] ORCID: 0000-0001-6362-9496, znamen@phys.msu.ru
[3] ORCID: 0000-0002-6545-5829, muratov583@gmail.com
[4] ORCID: 0009-0008-3233-0043, iz1721@mail.ru

Abstract

The velocity and temperature fields of an incident shock wave boundary layer interaction region for a flat plate flow is investigated. The research was carried out on a supersonic wind tunnel of periodic action with a closed working part and an adjustable supersonic nozzle, and impulse shock tube with flow duration up to several milliseconds. The shock system was generated by a wedge mounted at a distance of 20 mm from the upper wall, and by local inhomogeneities of the channel. The thickness of the boundary layer at the beginning of the test section on the upper and lower walls was about 6 mm. Experimental channels are equipped with optical quartz side windows and transparent upper and lower plexiglass sections, which allows the use of panoramic visualization methods. The distribution of the longitudinal and transverse components of the flow velocity in the interaction region of the incident shock wave with a flat plate was determined using the PIV method. The flow pattern in the area of interaction of the incident shock wave with the wall was also visualized using infrared thermography and the IAB-451 shadow device.

Keywords: wind tunnel, shock tube, shadow method, shock wave, boundary layer, PIV, infrared thermography.

1. Introduction

The study of shock wave interactions with boundary layers on various surfaces is a classic problem in gas dynamics. Research in this area has been ongoing for over 70 years [1]. However, many questions remain unresolved. When shock waves propagate in channels, complex wave system is formed due to the geometric features of the channels and local surface imperfections. Geometric features include variable channel cross-sections, the presence of shock wave generators (e.g., wedges, steps), and energy dissipation sources, such as those caused by impulsive effects. Even in channels with constant cross-sections and without macroscopic disturbances, flow perturbations arise due to interactions with local imperfections, such as wall roughness, gaps at section joints, and similar factors.

Under these conditions, the intensity of the incident shock wave decreases due to the dissipation of part of the main flow's kinetic energy in the axial direction and the redistribution of energy into transverse waves - compression waves [2]. Thus, in addition to viscous losses associated with boundary layer development on the walls, wave-induced energy dissipation also occurs. Consequently, key issues requiring special attention [3-5] include determining the location and magnitude of peak thermal and dynamic loads arising from shock wave interactions with various surfaces, as well as assessing the impact of perturbing factors on the state of the compressible gas flow. According to [6-8], further progress in modeling such in-

teractions is impossible without reliable experimental data on the distribution of gas-dynamic parameters in the regions of incident and interacting shock waves. Meanwhile, significant progress has been made in recent years in predicting heat transfer in laminar boundary layers using CFD models. However, challenges remain in modeling the separation of turbulent boundary layers and calculating flow around complex-shaped surfaces [9].

The use of panoramic measurement methods for studying high-speed flows, unlike traditional methods (e.g., anemometry, laser Doppler anemometry), offers several advantages [10, 11]. For instance, they allow for the measurement of instantaneous distributions of physical quantities, identification of coherent structures in the flow, and investigation of unsteady flows and fast processes. The most well-known panoramic method is Particle Image Velocimetry (PIV). In practice, panoramic infrared (IR) visualization methods are often used to assess heat fluxes on streamlined surfaces, enabling the identification of laminar-turbulent transition zones and regions of flow separation and reattachment [12].

The PIV method is an optical technique for measuring instantaneous velocity fields in a selected flow cross-section [13, 14]. A pulsed laser creates a thin light sheet to illuminate fine tracer particles suspended in the flow. The positions of these particles during two consecutive laser pulses are recorded in two frames by a digital camera. Flow velocity is determined by calculating the displacement of particles between the laser pulses. This displacement is calculated using correlation methods applied to tracer images, with the image divided into regular elementary regions. To improve measurement accuracy, statistics are collected from tens or hundreds of such frames, resulting in velocity vector fields across nearly the entire measurement area. A cross-correlation method is used to automate the processing of frame series, digitizing each frame by brightness (particles vs. background) and obtaining all possible matches for particle displacements between frames. The noise peak corresponding to the actual particle displacement is higher than other peaks representing alternative displacements.

The PIV method is widely used in gas dynamics studies of supersonic flows [15-20]. It enables the determination of two or even three (in the case of stereo-PIV) components of the flow velocity vector. However, its application in supersonic wind tunnels involves challenges, such as selecting appropriate tracers, choosing the seeding location along the facility's flow path, improving seeding uniformity, and mitigating parasitic laser illumination, among others.

IR thermography is an optical method for detecting infrared radiation from object surfaces, capable of converting this radiation into a panoramic temperature map [21]. In applied gas dynamics and heat transfer problems, IR thermography is primarily used to study heat fluxes on streamlined surfaces [22-24].

The aim of this work is to validate the use of panoramic optical PIV and IR thermography methods for studying the interaction of an incident shock wave with a turbulent boundary layer on a channel wall. Additionally, the obtained images were compared with those from the traditional shadow method.

2. Experimental Setup and Methodology

Experiments were conducted on the base of a supersonic wind tunnel with a closed test section and an adjustable supersonic nozzle (Fig. 1) (Experiment 1) [25, 26], as well as on the UTRO-3 impulse shock tube (Fig. 2) (Experiment 2) [27].

Experiment 1. The test section dimensions were: length – 200 mm, width – 70 mm, height – 98 mm. The Reynolds number, calculated based on the growth length of the dynamic boundary layer from the nozzle's critical section, was at least $2 \cdot 10^7$ at the nozzle exit, indicating turbulent flow conditions. The boundary layer thickness at the start of the test section on the upper and lower walls was approximately 6 mm. The setup was equipped with optical quartz side windows and transparent upper and lower plexiglass walls, enabling panoramic visualization methods.

In this study, the Mach number of the flow at the nozzle exit was $M_\infty = 2.74$. The critical nozzle section dimensions were 70×29 mm. A steel wedge with a 12° opening angle was in-

stalled on the upper wall of the test section before the plate to generate a shock wave (Fig. 1). The total pressure in the prechamber was 532 kPa, and the total temperature was 295.4 K.

In the first stage of the experiment, the side window of the test section was replaced with a ZnSe window, transparent in the infrared spectrum, allowing the temperature of the lower and side surfaces of the test section to be recorded using an InfraTEC IR8800 camera. Additionally, in this experiment, the lower wall of the test section could be heated from the back. The surface emissivity of the model was 0.9 (the wall was pre-blackened). The infrared transmission coefficient of the ZnSe window was 0.7.

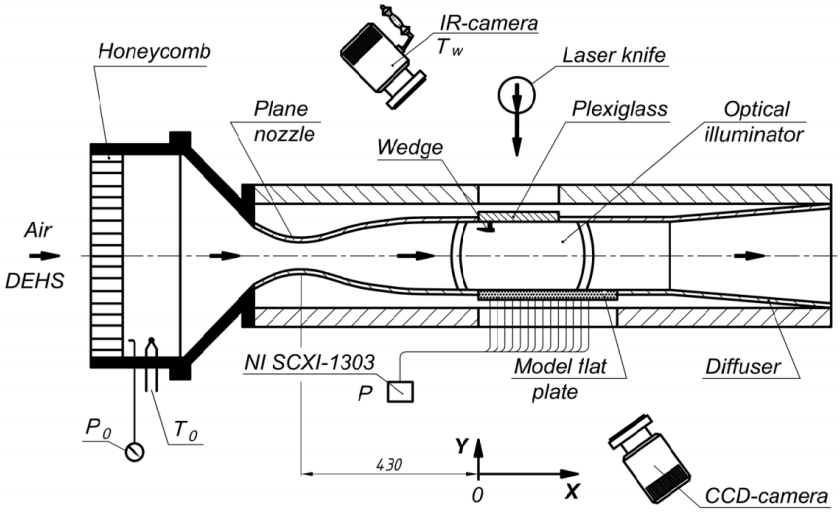

Fig. 1. The scheme of the supersonic wind tunnel

When using optical quartz side windows and a transparent plexiglass upper wall, PIV measurements could be conducted. The setup was equipped with a two-dimensional, two-component (2D2C) PIV system. The PIV system included an aerosol generator (Scitek, DEHS liquid), a flow illumination system based on a dual-pulse Nd:YAG laser (Beamtech, 532 nm wavelength), a CCD camera with a frame rate of up to 15 Hz at full resolution, and a Polis synchronizing processor [28]. The laser beam was expanded into a plane using a lens, creating a laser sheet along the model's centerline in the flow direction. The camera, positioned beside the test section, recorded tracer positions through the window during laser illumination.

Experiment 2. Thermographic studies of non-stationary heat fluxes on the side walls of the single-diaphragm UTRO-3 shock tube (Fig. 2 A). The Mach number of the incident shock wave varied in the range M = 3.1–3.6.

A uniform co-current flow in the test section lasted for several milliseconds. The maximum Reynolds number of the flow, estimated based on the channel width, was $Re \sim 10^5$. The shock wave propagation channel was 0.29 m long with an internal cross-section of 48×24 mm. Air and helium were used as the working and driving gases, respectively. At a distance of 0.2 m from the diaphragm rupture point, the test section was equipped with quartz windows (170 mm × 16 mm × 24 mm), transparent (transmission band 0.2 ÷ 2.8 μm) in the infrared range for the used thermal imager (operating range 1.5 ÷ 5.1 μm). This allowed recording the intensity of IR radiation from heated surfaces inside the channel (including the internal window surfaces) using the thermal imager.

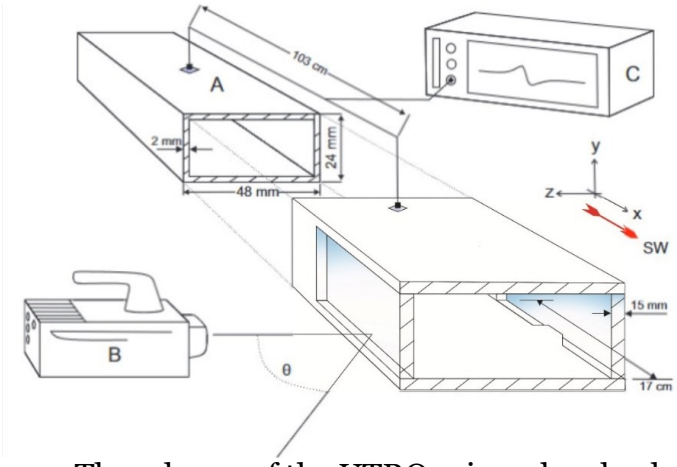

Fig. 2. The scheme of the UTRO-3 impulse shock tube

The Telops Fast M200 thermal imager (frame rate 1800 fps, exposure 200 μs) (Fig. 2 B) recorded integral heat fluxes from the inner surfaces of the quartz windows, corresponding to the thermal fields in non-stationary gas-dynamic flow. The interaction of the flow with the streamlined walls was depicted in the distribution of thermal fields on the heated channel walls, corresponding to the evolution of near-surface flow parameters [29]. The heat transfer process in this case was highly non-stationary and, depending on the thermophysical conditions, could occur in both directions—from the heated gas to the walls and vice versa. The resulting visualized thermal field distributions were obtained during the passage of a shock wave through a constant-cross-section channel and the subsequent formation of a system of oblique shock waves behind it, interacting with the quartz channel walls.

3. Experimental Results

Experiment 1.

Fig. 3 shows a shadow visualization capturing the interaction region of an incident shock wave with the boundary layer on a plate. The visualization clearly shows the incident and reflected shock waves, as well as the separation region. In the separation region, an additional compression shock wave forms due to the forward spread of the separation relative to the shock wave incidence area. At the nozzle exit, weak-intensity characteristic waves are observed.

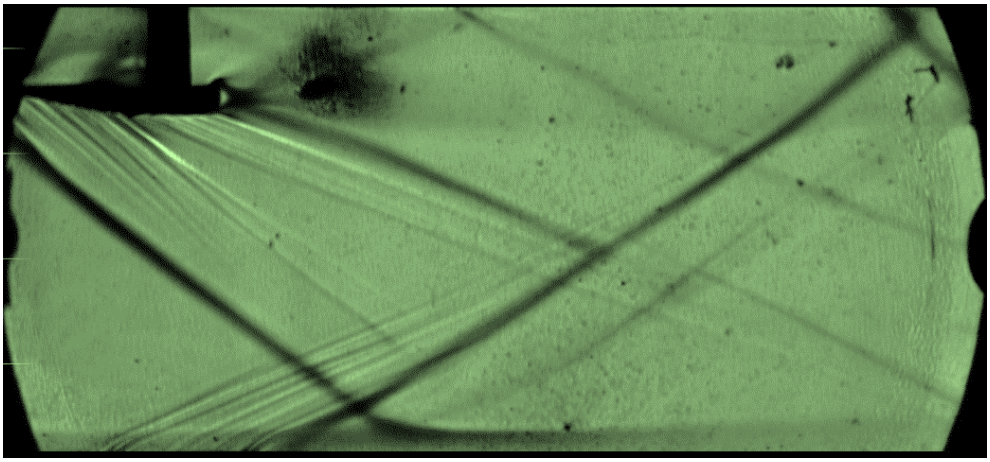

Fig. 3. Shadow visualization of an incident shock wave on a flat wall behind a wedge

Fig. 4 shows an instantaneous CCD camera snapshot from the PIV system. This visualization is essentially a shadow schlieren image capturing the interaction region of the incident shock wave with the boundary layer. Illumination was provided by a laser sheet from above, with partial reflection observed on the lower wall. The brightness range of the image (re-

quired for post-processing with the PIV cross-correlation algorithm) is indicated in the legend on the right. When the image is enlarged, illuminated tracers are visible across nearly the entire frame.

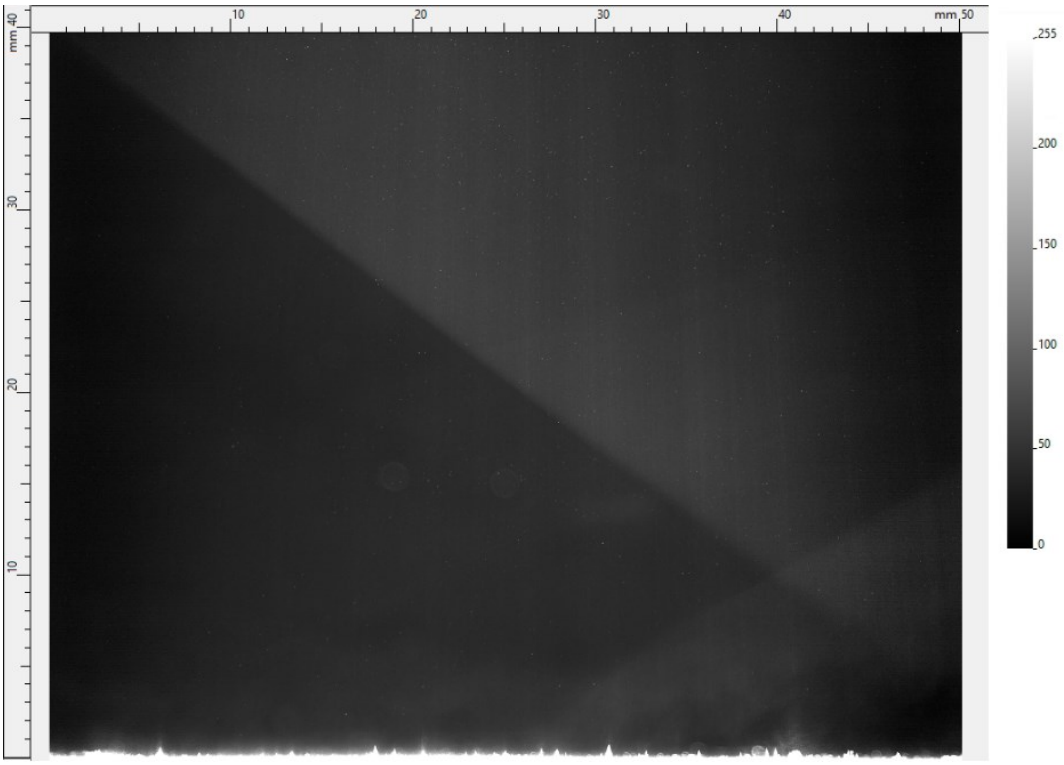

Fig. 4. Instantaneous CCD camera snapshot of the PIV system showing the interaction region of an incident shock wave with the boundary layer on a flat wall

Fig. 5 shows the result of cross-correlation processing of a series of paired images obtained in the experiment. The PIV method enables the determination of velocity distribution in the measurement area and visualization of the flow structures. The visualizations in Figs. 4 and 5 clearly show the incident and reflected shock waves, as well as the separation region. The Reynolds number, calculated based on the distance from the critical section to the nozzle exit, is approximately $2 \cdot 10^7$, indicating turbulent flow conditions. As the pressure gradient on the wall increases, the velocity profile becomes less filled, the boundary layer thickness increases, and separation and reverse flow zones are observed. Further downstream, the boundary layer reattaches to the wall. Fig. 5 also shows vectors of the longitudinal velocity component, indicating a characteristic flow turn behind the incident shock wave and straightening behind the reflected one.

Fig. 6 presents a thermogram of the interaction region of the incident shock wave with the lower channel wall. Similar to results obtained for an oncoming flow Mach number of 2.48 [20, 25], a temperature distribution on the wall is observed in the interaction region, with local extrema corresponding to boundary layer separation and reattachment. Downstream of the reattachment point, a local temperature increase is observed in the center of the channel, with areas of lower temperature in the corners, probably related to the development of secondary flows [31].

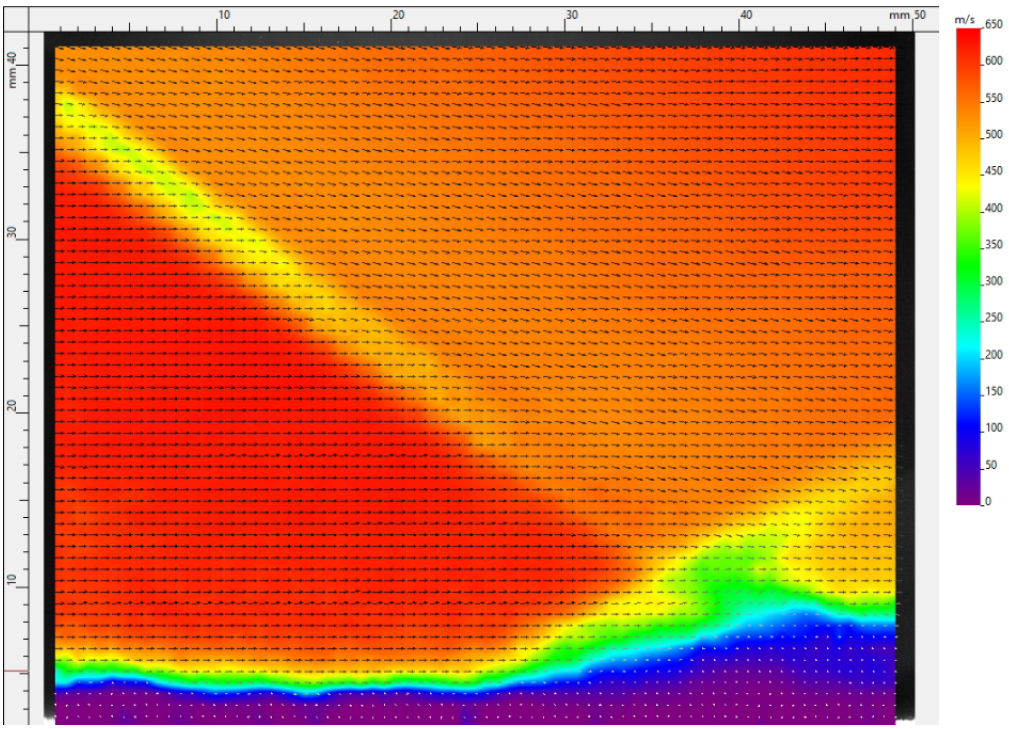

Fig. 5. PIV visualization of the interaction region of an incident shock wave with the boundary layer

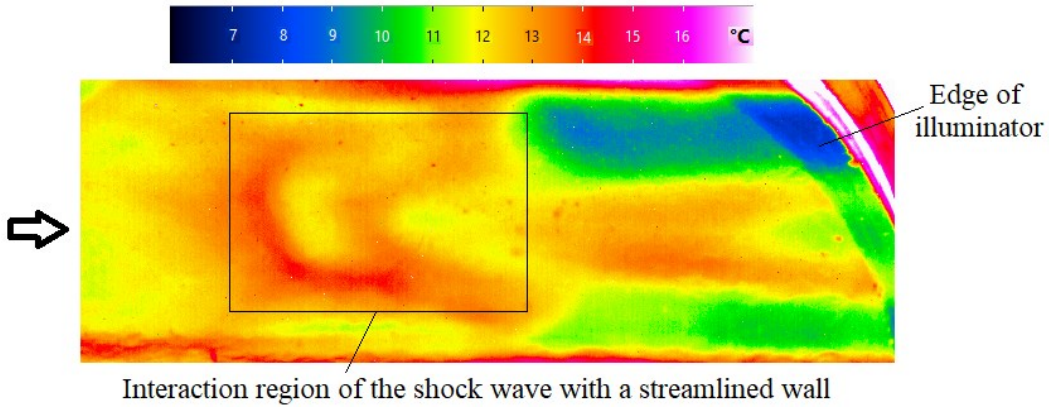

Fig. 6. Thermographic visualization of the incident shock wave interaction with the lower wall

Experiment 2.

Thermograms were obtained on the side quartz walls of the shock tube, corresponding to the distribution of thermal fields in the co-current flow behind the incident shock wave. A series of structures with varying radiation intensity are visualized, reflecting the gas-dynamic flow regions (Fig. 7). Thus, during the interaction of the shock wave with the joints of the shock tube channel sections, the flow structure is disturbed, forming a grid of planar oblique shock waves [2, 32]. The generated oblique shocks behind the incident wave reflect off the inner channel walls, creating a cascade of multiply reflected shocks downstream. During a quasi-homogeneous co-current flow (Mach number $M \sim 1.2$) in the channel, the resulting shock system is only slightly advected with the flow, changing its inclination relative to the channel as the main flow decelerates (after 400–500 μs). Over the camera's exposure time (200 μs), the transient heat exchange between the quartz sidewalls and the gas boundary layers is integrally visualized on the thermal map of the near-surface flow behind the shock wave, highlighting the system of oblique shocks.

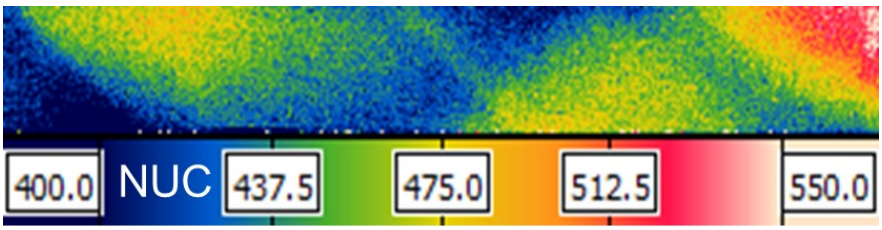

Fig. 7. Thermographic visualization of the interaction of a shock wave with M = 3.6 with the side wall of the testing section. The thermograms are presented in the NUC (Non-Uniformity Correction) scale, which is proportional to the radiation intensity from the studied region

Comparing longitudinal (Fig. 7) and transverse (Fig. 6) thermal patterns on the walls of flat channels formed by shock wave-boundary layer interactions, changes in thermophysical and dynamic loads along the channel can be determined [33].

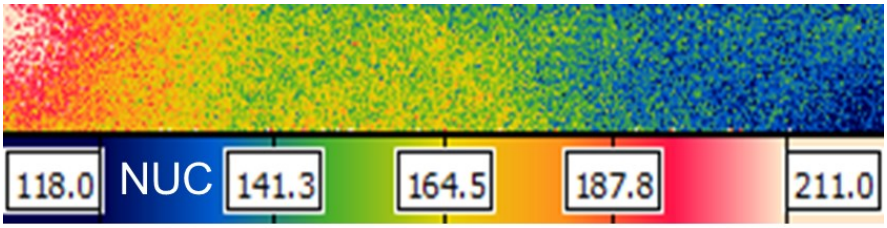

Fig. 8. Thermographic visualization of the interaction of a shock wave with M = 3.1 with the side wall of the testing section. The thermograms are presented in the NUC (Non-Uniformity Correction) scale, which is proportional to the radiation intensity from the studied region

As the intensity of the incident shock wave changes, the degree of gas compression, along with the corresponding density and temperature of the gas flow in compression and rarefaction regions, changes nonlinearly (Fig. 8). With an increase in the intensity of the incident shock wave, these processes lead to heat transfer enhancement between the gas medium and the channel wall – more intense integral thermograms are recorded, and the slope of the regions' boundaries changes. The sine of the envelope angle is inversely proportional to the Mach number of the incident shock wave:

$$sin(\alpha) \propto \frac{1}{M_\infty}$$

Thus, with a change in the velocity of the incident shock wave, a shift in extrema and a change in the loads amplitude on the channel walls should be expected. The estimated flow intensities in the channel, derived from the oblique shock system's angle, were $M_\infty \approx 1.2$ for an incident shock wave Mach number $M = 3.6$ and $M_\infty \approx 1.1$ for an incident shock wave Mach number $M = 3.1$.

4. Conclusion

The results of an experimental study of the interaction of an initiated shock wave with a turbulent boundary layer on a flat wall streamlined by a supersonic air flow with a Mach number M_∞ = 2.74 (Experiment 1 in the wind tunnel) and M_∞ = 1.1–1.2 (Experiment 2 in the shock tube) are presented. The shock wave was initiated by a wedge generator with a 12° opening angle and local imperfections in the shock tube channel. The wall static pressure distribution was measured through drainage holes on the model surface. The flow in the shock wave-boundary layer interaction region was visualized using shadow visualization, PIV, and infrared thermography methods. The flow velocity behind the incident shock wave in the wind tunnel channel decreased from 630 m/s in the oncoming flow to 540 m/s behind the shock wave. The separation zone length of the boundary layer reached 26 mm. The position of maximum static pressure corresponded to the boundary layer reattachment region down-

stream of separation. The zones of extreme thermal and dynamic loads on flat channel walls were visualized across two test benches (for steady-state and pulsed impact conditions).

Acknowledgments

The work is supported by the Russian Science Foundation (Grant N. 23-19-00096).

References

1. Dolling D.S. Fifty years of shock-wave/boundary-layer interaction research: what next? // AIAA J. 2001. Vol. 39. № 8. Pp. 1517-1531.

2. Bazhenova T.V., Gvozdeva L.G., Lagutov Yu.P., Lyakhov V.N., Faresov Yu.M., Fokeev V.P. Nonstationary Interactions of Shock and Detonation Waves in Gases // M: Nauka. 1986. [in Russian]

3. Gaitonde D.V. Progress in shock wave/boundary layer interaction // Prog. Aerosp. Sci. 2015. № 72. Pp. 80-99.

4. Huang W., Wu H., Yang Y.-g., Yan L., Li S.-b. Recent advances in the shock wave/boundary layer interaction and its control in internal and external flows // Acta Astronautica. 2020. № 174. Pp. 103-122.

5. Leontiev A.I., Lushchik V.G., Makarova M.S., Popovich S.S. Temperature Recovery Factor in a Compressible Turbulent Boundary Layer // High Temperature. 2022. Vol. 60. Pp. 409-431.

6. Knight D.D., Degrez G. Shock wave boundary layer interactions in high Mach number flows. A critical survey of current numerical prediction capabilities // Advisory Rept. 319, AGARD. 1998. № 2. Pp. 1-35.

7. Knight D.D., Yan H., Panaras A.G., Zheltovodov A.A. Advances in CFD prediction of shock wave turbulent boundary layer interactions // Prog. Aerosp. Sci. 2003. № 39. Pp. 121-184.

8. Doerffer P., Hirsch C., Dussauge J.-P., Babinsky H., Barakos G.N. Bump at a Wall (George Barakos). Unsteady Effects of Shock Wave Induced Separation. Springer Berlin Heidelberg, Berlin, Heidelberg, 2011. Pp. 13-53.

9. Neumann R.D., Freeman D.C. Experimental measurement of aerodynamic heating about complex shapes at supersonic Mach numbers // J. Spacecr. Rockets. 2012. № 49. Pp. 1080-1087.

10. Bilsky A.V., Gobyzov O.A., Markovich D.M Evolution and recent trends of particle image velocimetry for an aerodynamic experiment (review) // Thermophysics and Aeromechanics. 2020. Vol. 27. №. 1. Pp. 1-24.

11. Znamenskaya I.A. Methods for Panoramic Visualization and Digital Analysis of Thermophysical Flow Fields // Scientific Visualization. 2021. V. 13. N. 3. Pp. 125-158.

12. Carlomagno G.M., Cardone G. Infrared thermography for convective heat transfer measurements // Exp. Fluids. 2010. N. 49. Pp. 1187–1218.

13. Bilsky A.V., Gobyzov O.A., Markovich D.M., Kornilov V.I. Application of Digital Tracer Visualization Methods for Turbulent Boundary Layer Diagnostics // Thermophysics and Aeromechanics. 2012. Vol. 19. № 4. Pp. 401-413.

14. Raffel M., Willert C.E., Scarano F., Kähler C.J., Wereley S.T., Kompenhans J. Particle Image Velocimetry. A Practical Guide. 2018.

15. Humble R.W., Scarano F., van Oudheusden B.W. Experimental study of an incident shock wave/turbulent boundary layer interaction using PIV // AIAA. 2006. № 2006-3361. Pp. 1-16.

16. Scarano F. Overview of PIV in supersonic flows. In A. Schroeder, C.E. Willert (Eds.). Particle Image Velocimetry, Topics in Applied Physics. 2008. Vol. 112. Pp. 445-463.

17. Gobyzov O.A., Lozhkin Yu. A., Ganiev Yu. H., Krasenkov G. I., Larionov M. A., Nadezhdin A.E., Filippov P.S., Filippov S.E. Application of PIV for flow investigation in su-

personic wind tunnels // Proc. of the 12th Optical Methods of Flow Investigation International Conference. M: MPEI. 2013. [in Russian]

18. Ganiev Yu.Kh., Gobyzov O.A., Gusarova O.D., Zakharov E.P. Features of the Methodology for Experimental Non-Contact Diagnostics of Non-Uniform Velocity Fields in a Medium-Scale Supersonic Wind Tunnel // Proc. of the 3rd Industry Conference KIMILA. Zhukovsky: TsAGI, 2018. Pp. 302-311. [in Russian]

19. Egorov K.S., Zagaynov I.A., Popovich S.S. Experimental Development of a Panoramic Particle Image Velocimetry Method for Supersonic Wind Tunnel Studies // Proc. of the Future of Russian Mechanical Engineering. Moscow: BMSTU. 2023. Pp. 12-16. [in Russian]

20. Popovich S.S., Zditovets A.G., Kiselev N.A., Vinogradov U.A. Experimental study of aerodynamic heating in the region of an incident shock wave boundary layer interaction // Acta Astronautica. 2025. Vol. 229. Pp. 804-813.

21. Vavilov V.P. Infrared Thermography and Thermal Control. M: Nauka. 2013.

22. Nakamura H. Spatio-temporal measurement of convective heat transfer using infrared thermography. Heat Transfer - Theoretical Analysis // Experimental Investigations and Industrial Systems. InTech. 2011.

23. Cardone G., Zaccara M., Edelman J. A general procedure for infrared thermography heat transfer measurements in hypersonic wind tunnels // International Journal of Heat and Mass Transfer. 2020. V 163.

24. Rataczak J., Running C., Juliano T. Verification of quantitative infrared ther mography heat-flux measurements // Exp. Therm. Fluid Sci. 2021. V. 121.

25. Kozlov P.V., Popovich S.S., Zditovets A.G., Zagainov I.A. Experimental research of heat fluxes in wind tunnels and shock tubes // Physical-Chemical Kinetics in Gas Dynamics. 2024. Vol.25.

26. Popovich S.S. Aerodynamic cooling of the wall in the trace of a supersonic flow behind a backward-facing ledge // Fluid Dynamics. 2022. Vol. 57. № 1. Pp. 57-64.

27. Dolbnia D.I., Doroshchenko I.A., Znamenskaya I.A., Muratov M.I. New Approaches to Visualization and Analysis of Flows in Shock Tubes // Moscow University Physics Bulletin. 2025. № 3.

28. Akhmetbekov Ye.K., Bilsky A.V., Markovich D.M., Maslov A.A., Polivanov P.A., Tsyryulnikov I.S., Yaroslavtsev M.I. Application of the "Polis" Laser Measurement System for Velocity Field Measurements in Supersonic Flow in Wind Tunnels // Thermophysics and Aeromechanics. 2009. Vol.16. № 3. Pp. 343-352.

29. Znamenskaya I.A., Muratov M.I., Karnozova E.A., Lutsky A.E. Heat Fluxes Visualization in High-Speed Flow behind the Shock Wave // Scientific Visualization. Vol. 15. № 3. Pp. 92-100.

30. Zhang Y., Tan H.J., Tian F.C., Zhuang Y. Control of incident shock/boundary-layer interaction by a two-dimensional bump // AIAA J. 2014. V. 52. Pp. 767–776.

31. Van Dyke M. An album of fluid motion // Parabolic Pr. 1982.

32. Znamenskaya I.A., Muratov M.I., Dolbnya D.I. IR-thermography studies of high-speed gas-dynamic flows // International Journal of Thermal Sciences. 2025. V. 214.